Optical Engineering

OpticalEngineering.SPIEDigitalLibrary.org

High-integrated spectral splitting solar concentrator with double-light guide layers

Hongcai Ma
Qingyu Meng
Shuyan Xu
Jihong Dong
Wei Li

SPIE.

High-integrated spectral splitting solar concentrator with double-light guide layers

Hongcai Ma,* Qingyu Meng, Shuyan Xu, Jihong Dong, and Wei Li
Chinese Academy of Sciences, Changchun Institute of Optics, Fine Mechanics and Physics, Dong-Nanhu Road 3888, Changchun 130033, China

Abstract. Individual secondary optical components in a spectral splitting solar concentrator utilizing a microlens array require multiple photovoltaic (PV) cells, which leads to the complexity of system alignment and a high cost. In order to improve the integration of the PV cells and thermal management, a spectral splitting concentrator coupled to double-light guide layers has been proposed. Using one-axis tracking, we further investigate the optical performance of the concentrator combined with a cylindrical microlens array with double vertically staggered light guide layers in detail. The results show that this solar concentrator maintains a good acceptance angle of ± 2 deg in the east-west direction and an acceptable angle of ± 14 deg in the perpendicular direction on both low and high spectrums, achieving a concentration ratio of 10×. Finally, the capability of lateral displacement tracking has been explored for an aperture angle of ± 24 deg in this concentrator. [DOI: 10.1117/1.OE.53.10.105102]

Keywords: geometric optical design; solar energy; nonimaging optics; concentrators.

Paper 140859 received May 29, 2014; revised manuscript received Aug. 10, 2014; accepted for publication Sep. 15, 2014; published online Oct. 27, 2014.

1 Introduction

With the promotion of solar energy utilization, solar concentrating technology which increases the energy collecting efficiency has been rapidly developed and photovoltaic (PV) cells are generally identified as the most important components in a concentrator photovoltaic (CPV) system to realize photoelectricity power conversion.[1] To convert a large portion of the incident solar spectrum, a series of PV cells have been constructed by layering semiconductors with different absorption characteristics, manufactured by complex and high-cost multijunction technology.[2] Therefore, spectral splitting technology with a low-cost multiple single-junction PV cells has more potential applications due to the low concentration ratio and high photoelectricity conversion efficiency. The single module using spectral splitting technology obtains a high photoelectricity conversion efficiency of $42.7 \pm 2.5\%$ combined with an optical efficiency of 93%.[3] However, the manufacture of every single module increases the system cost and individual secondary optical components require multiple PV cells with orthogonal arrangements, which results in the complexity of the system alignment.

To improve packaging and thermal management compared to orthogonal arrangements, a spectral splitting concentrator that does not require two-axis solar tracking has been proposed, where adjacent splitting facets redirect the transverse propagation beam of the respective splitting facet downward and interleaved cells on a single circuit board replace two cells in the orthogonal orientation.[4] To further reduce PV connection complexity and allow one heat sink to manage the entire system output, a spectral splitting concentrator coupled with a point focusing lens array is invented and injected facets which redirect the focused beam to the end of the plate are introduced in the plate. The boundary layer between the double-light guide layers contains dichroic coating.[5] But the dichroic coating must be designed for not only spectral selection, but also angle selection, which is a complicated process. For overcoming the problem of the above concentration approach, the light guide layers with vertically staggered injected facets can be used.[6,7] The staggered injected facets redirect the sunlight transverse in the light guide layers without any leaking due to the injection points or directing surfaces downstream. This design has the potential advantages of high integration of PV cells and thermal management for the spectral splitting concentrator. However, to the best of our knowledge, there has not been any research in this direction.

In order to integrate the vertically staggered light guide layers into the spectral splitting concentrator, a novel spectral splitting concentrator with double-light guide layers is proposed in this paper. Using one-axis tracking, we deal with the design and optimization of the spectral splitting concentrator with a cylindrical microlens array and double vertically staggered light guide layers in detail. Finally, the capability of the lateral displacement tracking in the proposed concentrator is also preliminarily verified and we improve the aperture angle of this concentrator by optimization of the cylindrical microlens.

2 Spectral Splitting Concentrating Approach

Solar concentrators coupled to a single-light guide layer with injected facets have been developed recently.[8,9] In this concentration approach, the incoming sunlight is collected by a mass of primary concentrators and directed to a single PV cell by the injected facets in the single-light guide layer. The injected facets redirect the sunlight by reflection, refraction, total internal reflection, and so on, and generally function as shown in Fig. 1(a). We name the single-light guide layer for which the injected facets connect the bottom plane

*Address all correspondence to: Hongcai Ma, E-mail: hongcma@hotmail.com

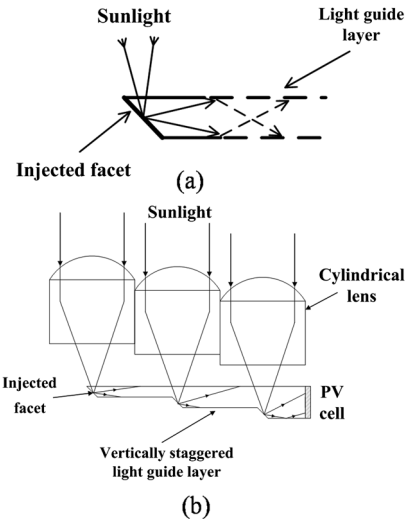

Fig. 1 Existing concentrating approach (side view). (a) Single-light guide layer, (b) concentrator with vertically staggered light guide layer.

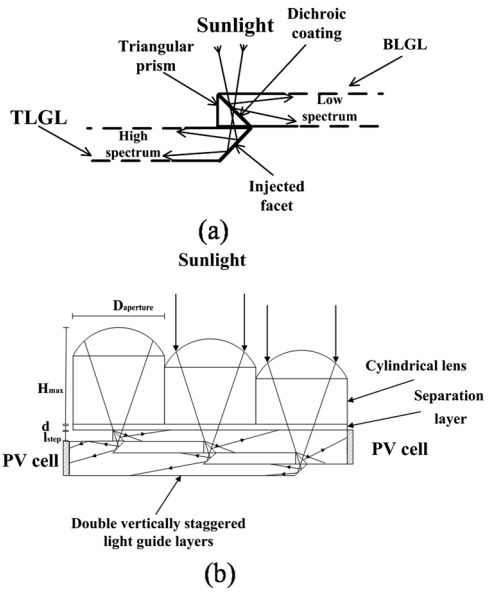

Fig. 2 Proposed spectral splitting concentrating approach (side view). (a) Double-light guide layers, (b) concentrator with double vertically staggered light guide layers.

as "bottom light guide layer (BLGL)" and the single-light guide layer for which the injected facets connect the top plane as "top light guide layer (TLGL)," respectively. Figure 1(b) shows the exiting concentrator combining a cylindrical lens array with a single-light guide layer with the vertically staggered injected facets, which can be extended in the longitudinal direction with a low manufacturing cost and can reduce the complexity of sun-tracking hardware.[6]

To integrate the single-light guide layer into the spectral splitting concentrator, we make the injected facets redirect the focused beam, while concurrently acting as spectral splitting facets. First, a BLGL is placed on a TLGL; then a dichroic coating is added to the injected facets in the BLGL and a triangular prism is also glued on the back of the dichroic coating; finally, the BLGL on the top is assembled with the TLGL on the bottom, thus constructing the double-light guide layers as shown in Fig. 2(a).

Furthermore, the spectral splitting concentrator combined a cylindrical microlens array with double vertically staggered light guide layers is proposed as shown in Fig. 2(b). Two single-junction PV cells are vertically located at the edges of the double-light guide layers. The primary cylindrical microlens receives the incoming sunlight and first transmits the sunlight toward the respective injected facets in the BLGL. The low spectrum remaining is reflected by the injected facets coated with a dichroic coating toward the respective single-junction PV cell suited for a low spectrum at the edge of the BLGL; the high spectrum is transmitted through the dichroic mirror toward the injected facets with a mirror in the TLGL and is then reflected toward the respective single-junction PV cell which is suited for the high spectrum at the edge of the TLGL. A low refractive index separation layer is selected and reduces Fresnel reflection losses due to the index differences between the material of the cylindrical microlens and the air.

In this spectral splitting concentrator, the cylindrical microlens array is selected as the primary concentrator and the microaperture results in a tiny spot size on the injected facet. The microlens array focus the incoming sunlight on the middle of the vertically adjacent injected facets and make the spot size minimum on the injected facets both in the BLGL and the TLGL. This concentrator with double-light guide layers keeps a compact and equal thickness between the top and bottom planes of the double-light guide layers.

Using one-axis tracking, the concentrators need to have an acceptance angle of about ± 2 deg of tracking tolerance in the east-west direction to track the Sun displacement and an acceptance angle of ± 9 deg in the north-south direction to cover the Sun displacement from 8:30 to 16:30,[10] where the acceptance angle of the concentrator is defined as the incident angle when optical efficiency reaches 90%. Therefore, the goals of our design are an acceptance angle of ± 2 deg of tracking tolerance from east to west and an acceptance angle of ± 9 deg from north to south on both the low and high spectrums, achieving a concentration ratio of 10×. The wide acceptance angle from north to south allows the system to only actively align with one-axis tracking during the peak hours of sunlight from 8:30 to 16:30.

3 Concentrator System Design and Performance

3.1 *System Characteristic*

In this chapter, the optical characteristic of a spectral splitting concentrator with a cylindrical microlens array and double vertically staggered light guide layers is analyzed. The concentration ratio of this concentrator is shown as follows:

$$C = \frac{D_{\text{aperture}}}{l_{\text{step}}} = \frac{n}{2 \cdot (f/\#) \cdot \tan \theta}, \tag{1}$$

where D_{aperture} is the aperture of a single-cylindrical lens in elevation, l_{step} is the thickness of the injected facets, n is the refractive index of the single-cylindrical lens, θ is the field-of-view (FOV) of the single-cylindrical lens, and $f/\#$ is the F number of the single-cylindrical lens, where

$$f = \frac{nr}{n-1}, \tag{2}$$

where f is the focal length of the single-cylindrical lens, and r is the radius of curvature of the single-cylindrical lens. From Eq. (1), it is concluded that when the size of the injected facets is thicker, the FOV of the cylindrical lens become wider, while the solar concentration ratio decreases.

When the incident angles of sunlight vary, the lateral displacement of the single-cylindrical lens spot is derived from Gauss imaging theory as the following equation:

$$L = \frac{f \tan\theta}{n} = \frac{r \tan\theta}{n-1}, \tag{3}$$

where L represents the lateral displacement of the lens spot, which is necessary for the design of the lateral displacement tracking of this concentrator in Sec. 3.3.3. The cylindrical lens with a spot displacement makes the focused sunlight from the injected facets, so a short focal length of the cylindrical lens is required.

Though the vertical displacement of the injected facets in the BLGL and TLGL compared to single-light guide layer leads to losses of decoupled sunlight, chromatic dispersion of the cylindrical lens material compensates the losses in a way. When the cylindrical lens focuses on the wide spectrum, defocus would occur in a different spectrum, which is beneficial for coupling sunlight by the injected facets. It is an expected condition that the cylindrical lens makes a low spectrum which is focused near the injected facets in the BLGL and, simultaneously, a high spectrum focused near the injected facets in the TLGL as shown in Fig. 3. The compensation effect of the chromatic dispersion has an optimal relation $l_{\text{step}} = f(\lambda_1) - f(\lambda_2)$, where $f(\lambda)$ represents the focal length of the cylindrical lens, λ_1 represents the center wavelength of the low spectrum, and λ_2 represents the center wavelength of the high spectrum. In the process of system optimization, we make the λ_0 of the central defocus area focus on the middle plane of the two injected facets and the λ_0 comes from the following equation:

$$f(\lambda_0) = \frac{f(\lambda_1) + f(\lambda_2)}{2} = \frac{[2n(\lambda_1)\cdot n(\lambda_2) - n(\lambda_1) - n(\lambda_2)]\cdot r}{2[n(\lambda_1)-1][n(\lambda_2)-1]}, \tag{4}$$

where $n(\lambda)$ represents the refractive index of the cylindrical lens. Equation (4) is also useful for the design of this concentrator in Sec. 3.2.

3.2 *System Process of Design and Simulation*

The optical performance of the spectral splitting concentrator with double vertically staggered light guide layers has been simulated in the ZEMAX ray tracing software. Simulations were used in AM1.5 sunlight where wavelengths ranged from 0.4 to 1.6 μm (Ref. 11) and the angular distribution representing the solar disk was not included. It is assumed that the incident flux radiations of solar parallel light are normalized to 1000 W/m^2.

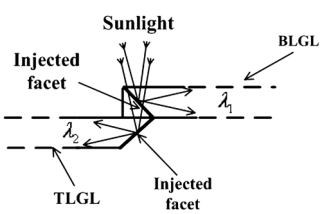

Fig. 3 Optimal compensation effect of chromatic dispersion.

The aperture of a single-cylindrical microlens was 5 mm and the cylindrical microlens array was arranged with a total amount of 10 in elevation. 0.5 mm of the thickness of the injected facets was derived from Eq. (1) according to the design goal of the concentration ratio. The thickness gradient of the adjacent cylindrical microlens in elevation equaled the thickness of the injected facets. The cylindrical microlens array selected BK7 ($n = 1.516$) material. Getting the optical efficiency consideration of Fresnel reflection losses on the lens surface, the cylindrical microlens array had an antireflection layer MgF_2 of 150 nm on the front surface.

Considering the absorption losses within the material, the material of the BLGL was adopted for high transmission though <855 nm and the material of the TLGL was adopted for high transmission through >855 nm. BK7 ($n = 1.516$) and F2 ($n = 1.62$) were selected for the BLGL and TLGL, respectively. Absorption losses become notable when the thickness of double-light guide layers increases vertically. A low refractive index separation layer with 0.2 mm of thickness and 1.42 of refractive index was inserted between the cylindrical microlens array and the BLGL, which ensures the sunlight transits in the BLGL by total internal reflection. The dichroic coating on the BLGL had a 45-deg surface and a cutoff at 855 nm. The current state-of-the-art in immersed 45-deg dichroic coatings is such that the average reflection of the dichroic coating from 400 to 800 nm was 98.2% (p-polarized 99.8%, s-polarized 96.0%) and the average transmission from 900 to 1800 nm was 97.9% (p-polarized 97.1%, s-polarized 99.3%).[12] In this paper, we assume that the average reflection of the dichroic coating from 400 to 855 nm was 98% (p-polarized 98%, s-polarized 98%) and the average transmission from 855 to 1600 nm was 98% (p-polarized 98%, s-polarized 98%). The TLGL also had 45-deg reflective surfaces on the respective injected facets, which were assumed to be ideal reflectors.

The process of optical design was as follows: first, according to Eq. (4), we made the wavelength of 750-nm focus on the middle plane of the two respective injected facets; then the approximate parameters of the cylindrical microlens were solved from Eq. (1) and set as the initializations in the optical software. To correct the inherent optical aberrations of the cylindrical microlens, the parameters of the lens with an aspheric radius of curvature, the conic, and the maximal thickness were optimized; finally, to allow the focal spot to be horizontally redirected as much as possible, the symmetric axis of the cylindrical microlens with respect to the middle axis of the unsymmetrical injected facets had a lateral displacement of 0.06 mm. The aspheric lens with a radius of curvature of 2.71 mm, conic of −0.437, and a maximal thickness of 7.3 mm was obtained. As a result, the spot of the aspheric cylindrical microlens at discrete angles up to 2 deg in elevation fall on the injected facets with a size of 500 μm. The general parameters of the concentrator are summarized in Table 1. The cross-sectional view of the proposed spectral splitting concentrator is illustrated in Fig. 4.

Table 1 General parameters achieved.

Parameter	Value
Radius of curvature of microlens (r)	2.71 mm
Conic constant of microlens (c)	−0.437
Aperture of microlens in elevation ($D_{aperture}$)	5 mm
Focal length of microlens (f)	5.24 mm
Maximal thickness of microlens (H_{max})	7.3 mm
Thickness of separation layer (d)	0.2 mm
Thickness of injected facets (l_{step})	0.5 mm
Aperture of concentrator	50×200 mm^2

3.3 *System Design Results*

3.3.1 *Acceptance angle of concentrator*

In this concentrator, the losses, including the Fresnel reflection in the front surface and the absorption inside the microlens material, are 0.2% and the absorption losses inside the double-light guide layers are 1.4% on the average. Figures 5(a) and 5(b) show the dependence of the incident angle of the optical efficiency in the proposed concentrator on the elevation and azimuth on both low and high spectra, respectively. From Fig. 5(a), this concentrator with a cylindrical microlens array keeps a good acceptance angle of ±2 deg of tracking tolerance with a 90% optical efficiency on both low and high spectrums in elevation; due to the limitation of the size of the injected facets, the focused beam begins to leak from the injected facets when the angle of incident sunlight is beyond ±2 deg and the optical efficiency falls off dramatically. When the angle of incident sunlight in elevation is beyond ±3 deg, the spot misses the injected facets in the double-light guide layers and the optical efficiency almost drops to zero. The curve of acceptance angle in elevation of this concentrator is so asymmetric because of the asymmetry of the injected facets. From Fig. 5(b), a wide acceptable angle of ±14 deg with a 90% optical efficiency and a large angle of ±22 deg with an 80% of optical efficiency were also obtained on both low and high spectra in azimuth. Otherwise, when the angle of incident sunlight is beyond ±14 deg in azimuth, the optical efficiency falls off slightly. The acceptable angle in the azimuth is much better than our previous goal, which depends on the longitudinal length of the cylindrical microlens. The above result of the simulation satisfies our goals of an acceptable angle of ±2 deg of tracking tolerance in elevation and an acceptable angle of ±9 deg in azimuth on both low and high spectra for one-axis tracking.

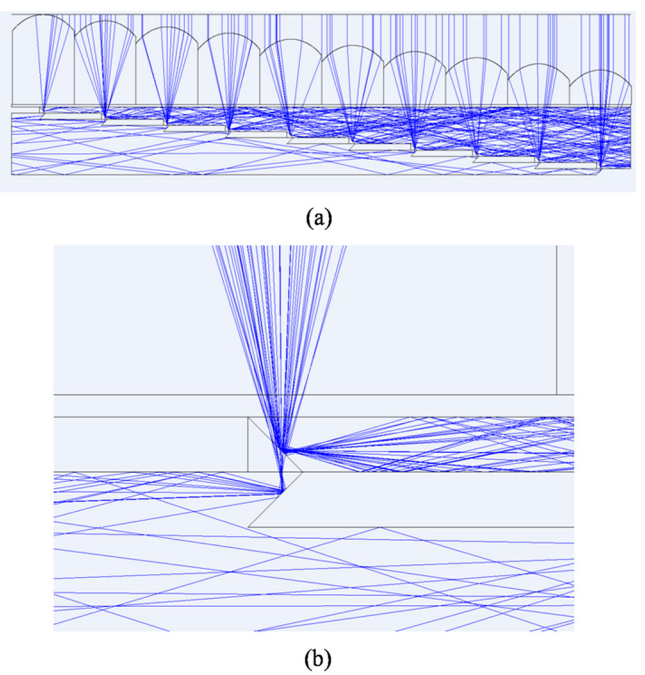

Fig. 4 Cross-sectional view of the proposed spectral splitting concentrator. (a) Concentrator with vertically staggered injected facets, (b) injected facet.

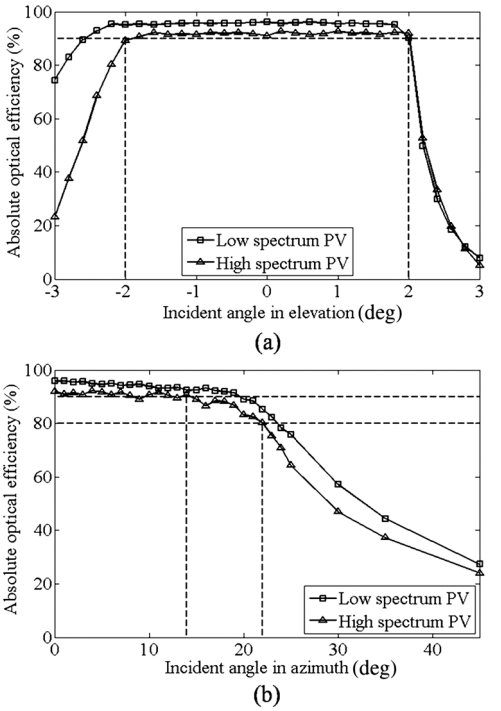

Fig. 5 Dependence of incident angle on optical efficiency (a) in elevation, (b) in azimuth.

3.3.2 *Flux radiations sub-PV cells received*

In the proposed spectral splitting concentrator, the receiver consists of two single-junction PV cells. The nonuniform illumination of a PV cell may produce a dramatic decrease of its solar-to-electric power conversion efficiency.[13] In this chapter, we analyze the flux radiations that the sub-PV cells received. Figures 6(a) and 6(b) show that in the case of on-axis sunlight incidence, the flux radiation is distributed over an area of 5×5 mm^2 on both the low and high spectra, respectively, where the unit is W/cm^2.

From Fig. 6(a), the maximum regional flux radiation on the low spectral PV cell is 1.335 W/cm^2 and the average flux radiation is 0.74804 W/cm^2, corresponding to 17.1 of the maximum regional concentration ratio and 9.6 of the average concentration ratio; from Fig. 6(b), the maximum

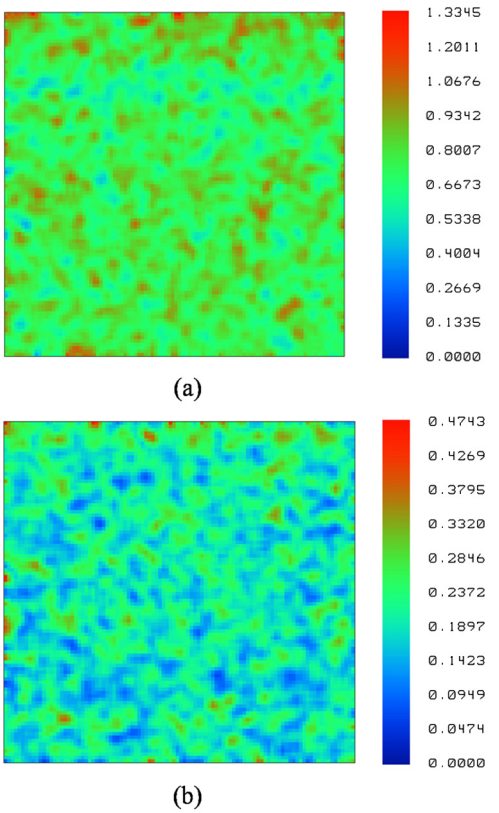

Fig. 6 Flux radiations of the area of 5×5 mm^2 with on-axis sunlight incidence (a) on the low spectral photovoltaic (PV) cell, (b) on the high spectral PV cell.

regional flux radiation on the high spectral PV cell is 0.4743 W/cm^2 and the average flux radiation is 0.2019 W/cm^2, corresponding to 21.6 of the maximum regional concentration ratio and 9.2 of the average concentration ratio. The average concentration ratio in consideration of the absorption losses and Fresnel reflection is approximately 10× of our design goal. Obviously, because of the repeated reflection of coupled sunlight in the double-light guide layers, the deviations of the flux radiation distribution on the area of 5×5 mm^2 on both low and high spectra is moderate. Compared to the point focus concentrator, the two sub-PV cells of the proposed spectral splitting concentrator receive good uniform radiation, which is beneficial to the photoelectricity conversion efficiency of the PV cells.

3.3.3 *Exploration of lateral displacement tracking*

The acceptable angles of most CPV systems are restricted because the optical axis must always remain parallel to the sun. Conventional sun-tracking hardware controls the whole CPV system, which is rotated to track the sun. This has the disadvantages of huge volume, complex configuration, and energy consumption. Lateral displacement tracking utilizes the lateral displacement between the primary concentrator and light guide layer to track the sun, which avoids utilizing the huge volume mechanical tracking equipment and reduces the complexity of the sun-tracking hardware.[14]

In this paper, we first apply the lateral displacement tracking in the concentrator with vertically staggered light guide layers and explore the capability of lateral displacement tracking. We make the cylindrical microlens array laterally displace relative to the double-light guide layers to track the sun, which approximately equals to the lateral displacement distance of the spot of the cylindrical lens. Taking 5 deg of parallel sunlight incidence in elevation as an example, the strategy of the proposed spectral splitting concentrator with lateral displacement tracking is illustrated in Fig. 7. We analyze the aperture angle of this concentrator covering up to ±24 deg with a polar aligned single-axis tracker.[15]

Before simulating the optical performance of this concentrator with lateral displacement tracking, the lateral displacement distances of the spot are derived from Eq. (3). Figure 8 shows the dependence of the incident angle in elevation on the optical efficiency with lateral displacement tracking on both low and high spectra. With the incident angle of sunlight from about −5 deg to 5 deg, the concentrator keeps a good 90% optical efficiency, however, when the incident angle of the sunlight continues to increase, the optical efficiency of this concentrator begins decreasing. There are two intrinsic reasons for the above results: while the off-axis aberrations of the microlens increase with FOV widening, the spot size of a wide FOV become larger, which results in leaking of the sunlight from the tiny injected facets; on the other hand, because of imaging distortion, the actual lateral displacement distance of the spot encircled energy deviates from the ideal lateral displacement distance from Eq. (3), which also decreases the optical efficiency of the sunlight of the injected facets.

Figure 9 shows the relationship between optical efficiency and incident angle with respect to 10 deg with lateral displacement tracking on both low and high spectra. The optical efficiency in elevation does not achieve 90%. It does remain above 60% from −2 deg to 2 deg with respect to 10 deg. Compared to a good tracking tolerance with respect to 0 deg, the tracking tolerance with respect to 10 deg slightly degenerates. We conclude that the tracking tolerance of the incident angles with respect to 0 deg and 10 deg with lateral displacement tracking are moderate.

The optical efficiency of the proposed concentrator with an aperture angle from −24 deg to 24 deg in elevation cannot achieve 90% and is not sufficient for the lateral displacement tracking. The optical efficiency in the full aperture angle can be further increased and balanced by optimization. Compared to the former system, we only optimize the parameters of a cylindrical microlens to enhance the aperture

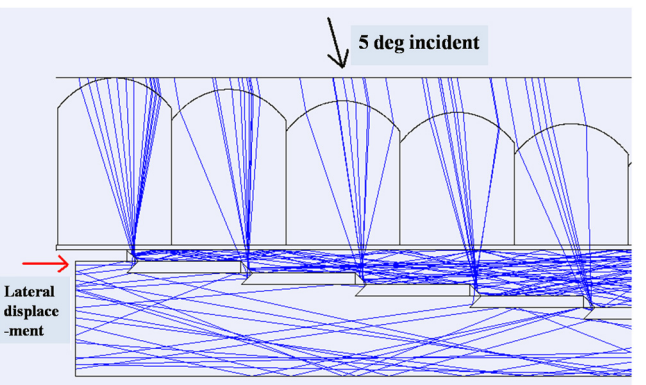

Fig. 7 Lateral displacement tracking with 5 deg of parallel light incidence in elevation.

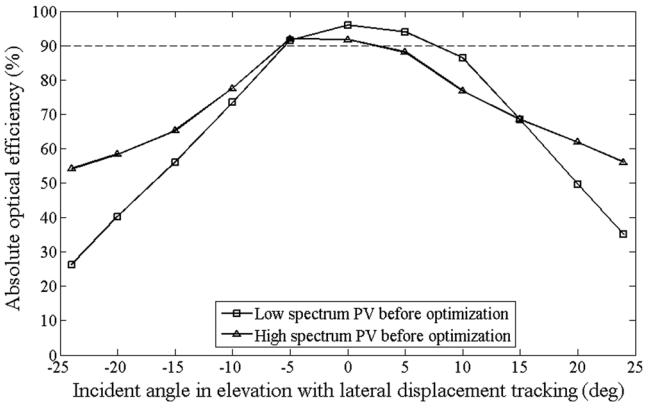

Fig. 8 Dependence of incident angle in elevation on optical efficiency with lateral displacement tracking.

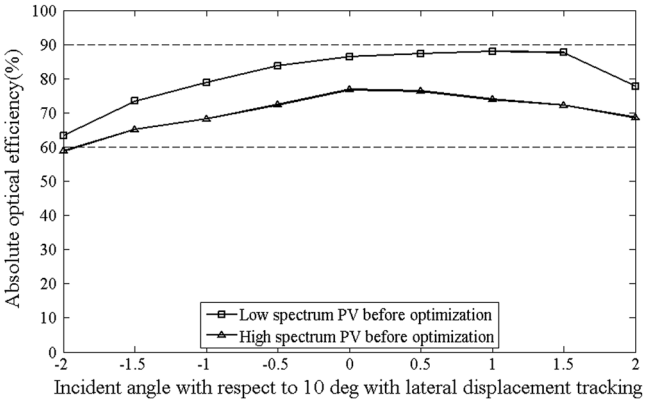

Fig. 9 Relationship between optical efficiency and incident angle with respect to 10 deg with lateral displacement tracking.

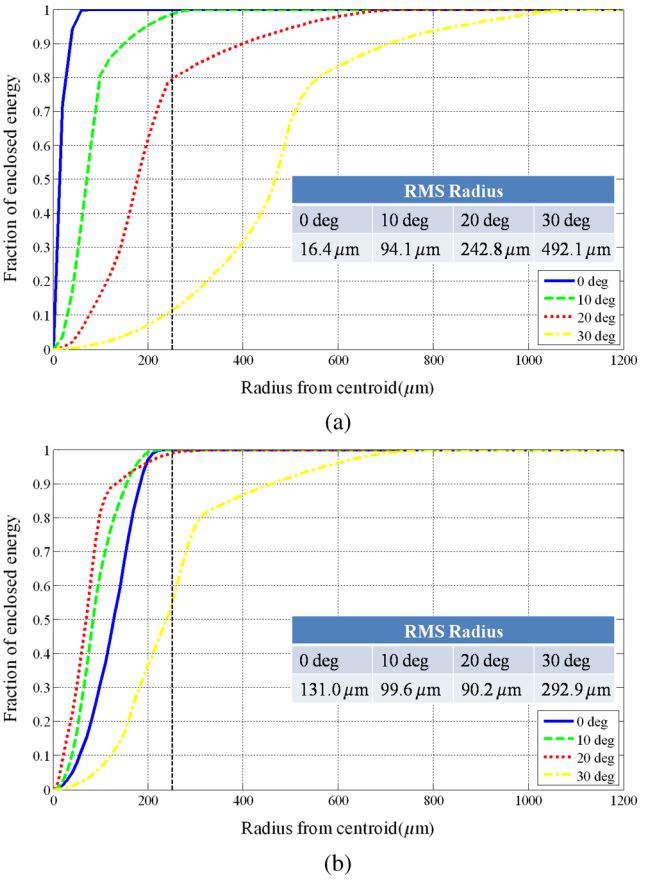

Fig. 10 Plots of encircled energy versus radius from centroid for (a) the former microlens, (b) the microlens optimized for field-of-view of 24 deg. The dashed line at 250 μm corresponds to the size of the injected facets.

angle of this concentrator. As a result, the aspheric cylindrical lens with a radius of curvature of 5.743 mm, conic constant of −0.447, and the maximal thickness of 15 mm were obtained. We quantify the widening of the off-axis focal spot for the former microlens and the microlens optimized for a FOV of 24 deg. The plots of the encircled energy versus the radius from the centroid for the former microlens and the microlens optimized for a FOV of 24 deg are shown in Figs. 10(a) and 10(b), respectively. The former microlens optimized only for a FOV of 2 deg achieves a smaller spot size of about 16.4 μm in the on-axis FOV. The spot size enlarges dramatically from 16.4 to 492.1 μm when the FOV increases from 0 deg to 30 deg. The fraction of the enclosed energy is only 80% on the injected facets with a FOV of 20 deg and drops to about 10% with a FOV of 30 deg. In addition, we analyze the performance of the microlens optimized for the FOV of 24 deg. The spot size in various FOVs is balanced after optimization of the single-cylindrical microlens. The fraction of the enclosed energy is about 95% on the injected facets with a FOV of 20 deg and is above 50% with a FOV of 30 deg.

Figure 11 shows the dependence of the incident angle in elevation with the optical efficiency with lateral displacement tracking on both low and high spectra after optimization. This concentrator maintains a good 90% of the optical efficiency from −15 deg to 15 deg in elevation while remaining above 60% in optical efficiency beyond ±15 deg. Obviously, the

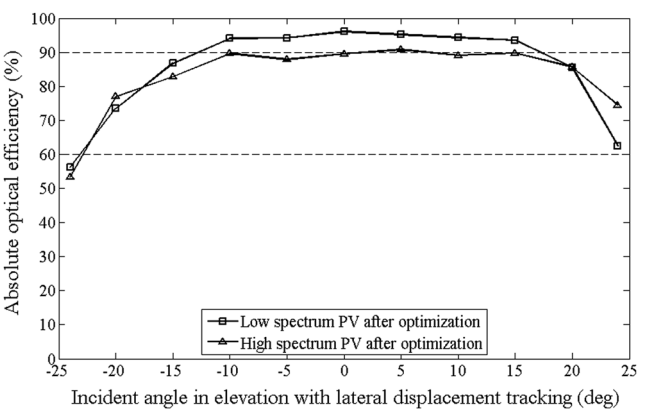

Fig. 11 Dependence of incident angle in elevation on optical efficiency with lateral displacement tracking after optimization.

performance of this concentrator with lateral displacement tracking is improved after optimization. Additionally, the glass material of the cylindrical microlens and light guide layers could be further optimized to improve the aperture angle.

We still analyze the tracking tolerance of the concentrator with lateral displacement tracking after optimization. Figures 12(a) and 12(b) show the relationship between the optical efficiency and incident angles with respect to 0 deg and 10 deg with lateral displacement tracking on both low

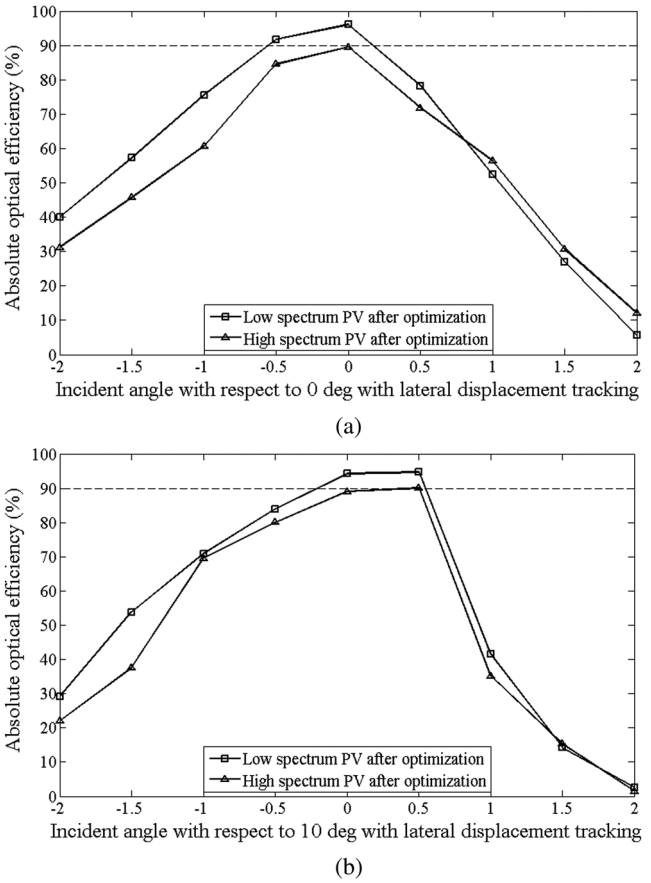

Fig. 12 Relationship between optical efficiency and incident angle with lateral displacement tracking (a) with respect to 0 deg, (b) with respect to 10 deg.

and high spectra, respectively. The optical efficiency in elevation remains 90% only near 0 deg and 10 deg, while the optical efficiency drops off rapidly when the incident angle of sunlight increases. It implies that the tracking tolerances of the concentrator after optimization are only approximately ± 0.2 deg and cannot reach ± 2 deg with respect to 0 deg and 10 deg.

Generally speaking, compared to the concentrator with lateral displacement tracking before optimization, the aperture angle of the concentrator is enhanced from ± 5 deg to ± 15 deg after optimization, while the tracking tolerances are about ± 0.2 deg with respect to 0 deg and 10 deg and become much lower, however, with an approximately ± 0.27 deg of the divergence angle of the sun. A wide aperture angle of ± 24 deg and a good tracking tolerance of ± 2 deg are not given considered. About ± 0.27 deg of tracking tolerance is preferable in this concentrator for lateral displacement tracking.

4 Conclusions

The proposed spectral splitting concentrator with a cylindrical microlens array and double vertically staggered light guide layers maintains a good acceptance angle of ± 2 deg in elevation and a large acceptance angle of ± 14 deg in azimuth for both low and high spectra for one-axis tracking, with a thickness of only 13 mm, achieving a concentration ratio of 10×. The aperture angle of this concentrator with lateral displacement tracking is enhanced from ± 5 deg to ± 15 deg by optimization, while the tracking tolerance is about ± 0.2 deg with respect to 0 deg and 10 deg, which is approximately ± 0.27 deg of the divergence angle of the sun. In comparison with the conventional spectral splitting concentrator with individual secondary optical components, the novel spectral splitting concentrator with double-light guide layers has the advantages of high integration of PV cells connection, united thermal management and a uniform flux radiation received. Further research will enhance the concentration ratio by adding a secondary concentrator such as a compound parabolic concentrator and tapper light guide layers.

References

1. A. Luque et al., *Solar Cells and Optics for Photovoltaic Concentration, Series on Optics and Optoelectronics*, Taylor & Francis, Bristol (1989).
2. A. Luque and S. Hegedus, Eds., *Handbook of Photovoltaic Science and Engineering*, 2nd ed., pp. 314–364, John Wiley & Sons, Ltd., West Sussex (2011).
3. A. Barnett et al., "Very high efficiency solar cell modules," *Prog. Photovolt.: Res. Appl.* **17**(1), 75–83 (2009).
4. J. H. Karp and J. E. Ford, "Multiband solar concentrator using transmissive dichroic beamsplitting," *Proc. SPIE* **7043**, 70430F (2008).
5. J. E. Ford et al., "System and method for solar energy capture and related method of manufacturing," US Patent No. 0226332 A1 (2011).
6. D. Moore, G. Schmidt, and B. Unger, "Concentrated photovoltaic stepped planar light guide," in *International Optical Design Conf., OSA Technical Digest (CD)*, paper JMB46P (2010).
7. S. Ghosh and D. S. Schultz, "Compact optics for concentration aggregation and illumination of light energy," US Patent No. 7664350 B2 (2010).
8. J. H. Karp et al., "Planar micro-optic solar concentrator," *Opt. Express* **18**(2), 1122–1133 (2010).
9. J. C. M. Anton et al., "Light collection and concentration system," US Patent No. 0116336 A1 (2010).
10. S. Bounchard and S. Thibault, "Planar waveguide concentrator used with a seasonal tracker," *Appl. Opt.* **51**(28), 6848–6854 (2012).
11. NREL, "AM1.5G solar spectrum irradiance data," http://rredc.nrel.gov/solar/spectra/am1.5/.
12. J. D. McCambridge et al., "Compact spectrum splitting photovoltaic module with high efficiency," *Prog. Photovolt.: Res. Appl.* **19**(3), 352–360 (2011).
13. R. Winston, J. C. Miñano, and P. Benitez, in *Nonimaging Optics*, N. Shatz and J. C. Bortz, Eds., pp. 318–327, Elsevier Academic, New York (2005).
14. J. M. Hallas et al., "Two-axis solar tracking accomplished through small lateral translations," *Appl. Opt.* **51**(25), 6117–6124 (2012).
15. F. Duerr, Y. Meuret, and H. Thienpont, "Tracking integration in concentrating photovoltaics using laterally moving optics," *Opt. Express* **19**(S3), A207–A218 (2011).

Hongcai Ma received his BS degree in physics from Jilin University in 2008 and his PhD degree in optical engineering from the Changchun Institute of Optics, Fine Mechanics and Physics, Chinese Academy of Sciences (CIOMP) in 2013. He is an assistant professor at the CIOMP now. His current research interests focus on nonimaging optics, solar concentrators, and space solar energy utilization.

Biographies of the other authors are not available.